Letter

Element-Specific Detection of Sub-Nanosecond Spin-Transfer Torque in a Nanomagnet Ensemble

Satoru Emori,* Christoph Klewe, Jan-Michael Schmalhorst, Jan Krieft, Padraic Shafer, Youngmin Lim, David A. Smith, Arjun Sapkota, Abhishek Srivastava, Claudia Mewes, Zijian Jiang, Behrouz Khodadadi, Hesham Elmkharram, Jean J. Heremans, Elke Arenholz, Günter Reiss, and Tim Mewes

Read Online

ACCESS | Metrics & More | Article Recommendations | SI Supporting Information

ABSTRACT: Spin currents can exert spin-transfer torques on magnetic systems even in the limit of vanishingly small net magnetization, as recently shown for antiferromagnets. Here, we experimentally show that a spin-transfer torque is operative in a macroscopic ensemble of weakly interacting, randomly magnetized Co nanomagnets. We employ element- and time-resolved X-ray ferromagnetic resonance (XFMR) spectroscopy to directly detect subnanosecond dynamics of the Co nanomagnets, excited into precession with cone angle $\gtrsim 0.003°$ by an oscillating spin current. XFMR measurements reveal that as the net moment of the ensemble decreases, the strength of the spin-transfer torque increases relative to those of magnetic field torques. Our findings point to spin-transfer torque as an effective way to manipulate the state of nanomagnet ensembles at subnanosecond time scales.

KEYWORDS: *spin-transfer torque, ferromagnetic resonance, spin pumping, magnetic nanoparticles, X-ray magnetic circular dichroism*
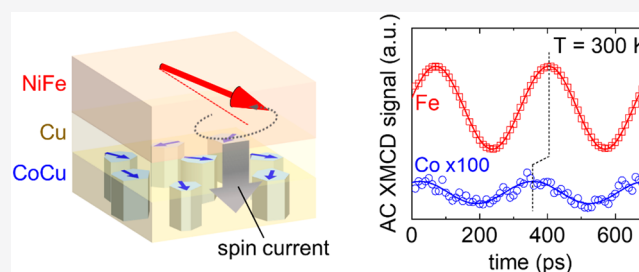
A flow of spin angular momentum, or spin current, injected into a thin-film magnetic medium can exert a spin-transfer torque (STT) on the magnetization.[1−3] STT enables a variety of scalable and energy-efficient nanoscale ferromagnetic devices for computing and communications applications.[4−7] Furthermore, STT can efficiently rotate the magnetic order of materials with zero net moment. For instance, STT (in particular, spin−orbit torque) allows for Néel vector switching[8,9] and auto-oscillations[10,11] in antiferromagnets. The net magnetization also averages to zero in a thermally disordered ensemble of weakly interacting ferromagnetic (or superparamagnetic) nanoparticles, particularly in the absence of an applied magnetic field. While examining the magnetization state of an antiferromagnet generally remains a challenge, ferromagnetic nanoparticles can be readily probed by conventional magnetometry, transport, and optical techniques. Thus, an ensemble of weakly coupled nanomagnets serves as a convenient experimental system for direct studies of the fundamental nature of STT in the limit of vanishing net magnetization. Such basic studies may provide insights into how to efficiently control the state of nanomagnetic ensembles, potentially for applications in probabilistic[7,12,13] and quantum[14,15] computing by means other than magnetic field pulses.

Here, we consider a fundamental distinction between STT and a torque generated by a magnetic field in such a nanomagnet ensemble, particularly on a sufficiently short time scale. Although a large fraction of the nanomagnet moments can relax (align) along a moderate field of ~0.1−1 T,

this relaxation process involves a finite time scale, for example, a few nanoseconds governed by the Gilbert damping rate.[16] On a shorter time scale, the moment $\mathbf{m}_i$ of each nanomagnet precesses about the field $\mathbf{H}$, as $\mathbf{m}_i$ is driven by the precessional torque $\tau_H \propto -\mathbf{m}_i \times \mathbf{H}$. This field-driven precessional torque sums to zero in the limit of vanishing total magnetization (Figure 1a), which is the case for a thermally disordered ensemble. By contrast, a spin current with polarization $\mathbf{s}$ exerts an STT of the form $\tau_{ST} \propto \mathbf{m}_i \times \mathbf{s} \times \mathbf{m}_i$,[1−3] which yields a finite sum even when the ensemble has zero net magnetization (Figure 1b). Thus, on a subnanosecond time scale, STT can yield a nonvanishing global torque in a nanomagnet ensemble with null net moment, whereas the precessional field torque alone cannot.

Prior experiments have shown that STT can control the state of a single superparamagnetic nanoisland[17] or nanoscale junction,[7,18−20] as well as a nearly saturated ensemble of nanomagnets.[21−23] Yet, none has demonstrated STT in a macroscopic ensemble of nanomagnets in a near-zero net magnetization state (Figure 1b). In this Letter, we present
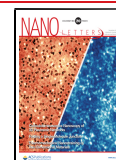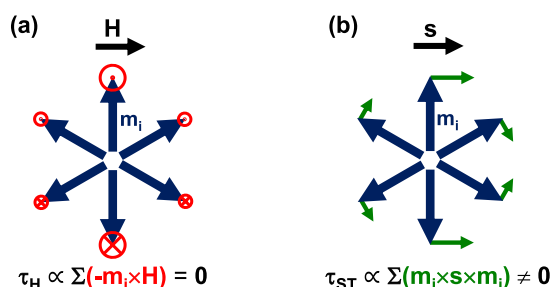
Figure 1. Illustrations of torques acting on an ensemble of magnetic moments, which sum to zero net magnetization, from (a) an externally applied field **H** and (b) spin current with polarization **s**.

experimental confirmation of a global STT in such an ensemble of weakly interacting, randomly magnetized nanomagnets. We perform spin pumping experiments[24−27] on a spin-valve-like film stack of NiFe/Cu/CoCu: the NiFe layer excited by microwave ferromagnetic resonance (FMR) pumps a coherent AC spin current that is absorbed by the granular CoCu spin sink, which consists of Co nanomagnets embedded in a nonmagnetic Cu-rich matrix.[28,29] The Co nanomagnets are collectively aligned at low temperature whereas their collective alignment is disordered at room temperature, thereby allowing us to compare the effect of STT on these two distinct global magnetic states. We employ the element- and time-resolved X-ray ferromagnetic resonance (XFMR) technique[27,30−36] to directly detect torques on the Co nanomagnet ensemble at the subnanosecond time scale. Whereas torques from the microwave and interlayer dipolar fields decrease sharply with increasing temperature (i.e., weaker collective alignment), a substantial global STT generated by the AC spin current survives in the nanomagnet ensemble. Our results point to STT as an effective way to drive an ensemble of nanomagnets at the subnanosecond time scale.

We employed DC sputter deposition with MgO substrates held at room temperature, resulting in polycrystalline films. Granular thin films of $Co_{25}Cu_{75}$ were grown by cosputtering Co and Cu targets; Co and Cu are immiscible, such that nanoscale Co granules segregate in the Cu-rich matrix.[28,29] The film composition was set by the Co and Cu deposition rates and corroborated by energy-dispersive X-ray spectroscopy. We estimated an average granule size of <16 nm in $Co_{25}Cu_{75}$ films from powder X-ray diffractometry.

We confirm the granular nature of single-layer 10 nm thick $Co_{25}Cu_{75}$ films. As shown in Figure 2a, our vibrating sample magnetometry measurements reveal room-temperature magnetization curves with zero coercivity and remanence. We observe similar magnetization curves for in-plane and out-of-plane field directions, indicating that static magnetic properties are not governed by the thin-film shape anisotropy. The nearly isotropic magnetization curves are consistent with isolated, weakly interacting Co granules embedded within the Cu-rich matrix, rather than a homogeneous solid solution of Co and Cu atoms.

The magnetic field dependence of resistance (Figure 2b) serves as additional evidence for the granular nature of the $Co_{25}Cu_{75}$ film. We observe a pronounced decrease in resistance R with increasing magnitude of magnetic field, with a magnetoresistance ratio of $|R(0) − R(1.4\ T)|/R(0) = |\Delta R|/R_0 \approx 2\%$ at room temperature. The magnetoresistance is similar for both in-plane and out-of-plane fields, consistent
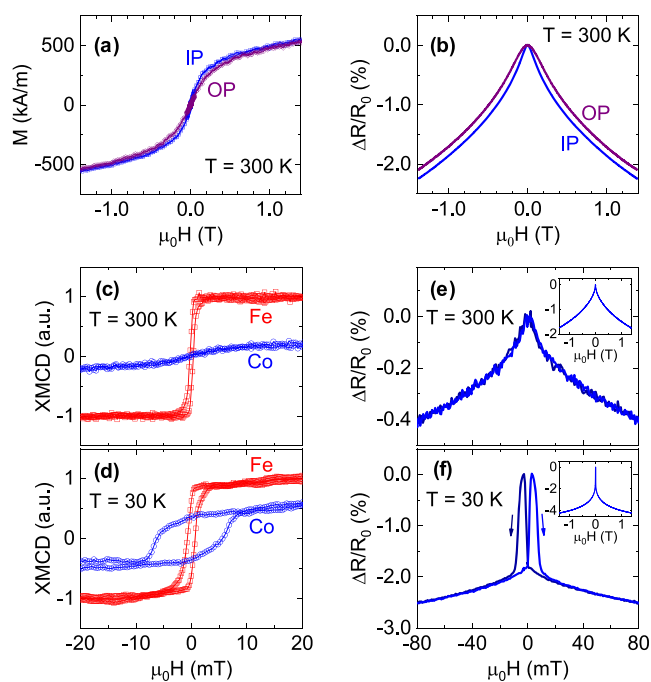

Figure 2. (a,b) Room-temperature in-plane (IP) and out-of-plane (OP) magnetization curves (a) and magnetoresistance curves (b) for single-layer $Co_{25}Cu_{75}(10)$. The magnetization in (a) is normalized by the estimated Co volume. (c,d) Element-resolved in-plane magnetization curves measured with XMCD for NiFe(10)/Cu(5)/CoCu(10) at (c) room temperature and (d) 30 K. (e,f) In-plane magnetoresistance curves for NiFe(10)/Cu(5)/CoCu(10) at (e) room temperature and (f) 30 K.

with previously reported isotropic giant magnetoresistance (GMR) in single-layer granular magnetic thin films.[28,29]

We have further examined static magnetic properties of the granular $Co_{25}Cu_{75}$ film in a spin-valve-like $Ni_{80}Fe_{20}(10)/Cu(5)/Co_{25}Cu_{75}(10)$ stack (thickness unit: nm) designed for our spin pumping experiment. By utilizing element-resolved X-ray magnetic circular dichroism (XMCD), separate magnetization signals are obtained for the NiFe layer from the Fe L_3 edge and the CoCu layer from the Co L_3 edge. As shown in Figure 2c,d, the NiFe and CoCu layers show qualitatively distinct field dependence, which verifies that the two layers are not exchange-coupled across the Cu spacer layer.[37] The room-temperature XMCD magnetization curve for CoCu shows zero remanence and coercivity, pointing to random alignment of the Co nanomagnets at low fields. By contrast, substantial remanence and coercivity are observed at lower temperatures (e.g., 30 K, Figure 2d), as thermal fluctuations are suppressed and the Co nanomagnets are able to align along the field collectively. The room-temperature magnetoresistance curve of the NiFe/Cu/CoCu stack (inset Figure 2e) is similar to that of single-layer CoCu (Figure 2b) and indicates that the CoCu layer in the NiFe/Cu/CoCu stack is also granular. Low-temperature magnetoresistance curves show finite coercivity (Figure 2f), consistent with the XMCD magnetization curve at the Co edge (Figure 2d). Overall, our results in Figure 2 corroborate the granular nature of $Co_{25}Cu_{75}$ and the reduced net magnetization of the ensemble with increasing temperature.

We now discuss the interplay of spin current and the Co nanomagnets in the NiFe/Cu/CoCu stack. We first look for evidence of the CoCu layer acting as a spin sink in broadband

FMR spin pumping measurements,[24−26] using a variable-temperature coplanar-waveguide spectrometer with the sample magnetized in the film plane. In these measurements, we detect and analyze the FMR signal from NiFe; the FMR signal from CoCu is negligibly small. From the linear slope of the NiFe FMR linewidth versus frequency (Figure 3a), we obtain the
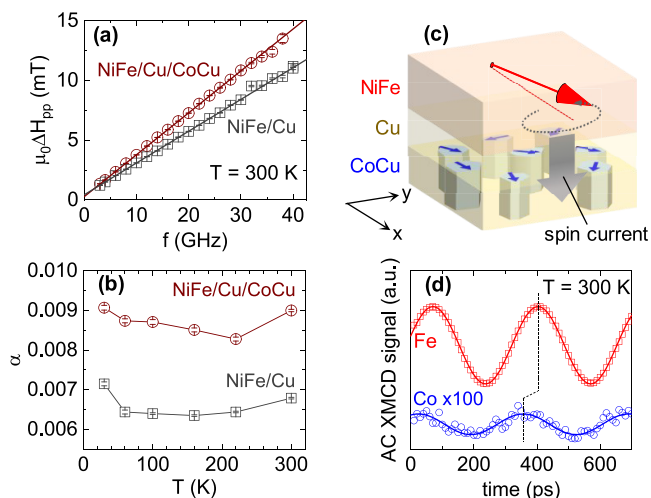

Figure 3. (a) Frequency dependence of the peak-to-peak FMR linewidth ΔH_{pp} for NiFe(10)/Cu(5)/CoCu(10) and control NiFe(10)/Cu(5) at room temperature. The solid lines show linear fits to obtain the Gilbert damping parameter. (b) Temperature dependence of the Gilbert damping parameter α. (c) Schematic of FMR spin pumping with NiFe as the spin source and Co nanomagnets as the spin sink. (d) Example of XFMR amplitude (AC XMCD) versus microwave delay for NiFe (Fe) and the nanomagnet spin sink (Co). The vertical dotted line emphasizes the offset in precessional phase.

Gilbert damping parameter α (see Supporting Information). At room temperature, α of the control sample without a CoCu layer is ≈0.007 in line with typical values for $Ni_{80}Fe_{20}$ (refs 38 and 39).

Compared to this control sample, the NiFe/Cu/CoCu sample exhibits α that is enhanced by ≈0.002 (+30%). The

magnitude of this damping enhancement is similar to prior results on spin-valve-like structures, where spin current is pumped from a NiFe layer and absorbed by another ferromagnetic layer.[26] The broadband FMR results thus suggest that granular CoCu acts as a sink for the spin current. We further observe that α is consistently greater by ≈0.002 for samples with the CoCu spin sink, independent of temperature (Figure 3b).

However, the broadband FMR measurements do not directly indicate whether the spin current generates any STT in the Co nanomagnet ensemble. To probe the magnetization dynamics of the Co nanomagnets, we have performed time- and element-sensitive XFMR measurements under a continuous-wave 3 GHz microwave field excitation. Details of the XFMR method can be found in the Supporting Information and refs 27 and 36. We emphasize that XFMR is a pump–probe technique that leverages XMCD to separately detect dynamics in the NiFe spin source (Fe L_3 edge) and the granular CoCu spin sink (Co L_3 edge). Specifically, we measured the oscillating magnetization (along the y-axis in Figure 3c) transverse to the externally applied DC field H_x (along the x-axis in Figure 3c) for each Fe and Co.

Figure 3d shows examples of XFMR pump–probe delay scans, acquired at room temperature and $\mu_0 H_x = 9.6$ mT close to the resonance field of NiFe. Sinusoidal oscillations are evident for both the NiFe layer and the Co nanomagnets. We comment on two key observations: (1) Because the X-ray beam spot has a diameter of ∼100 μm, the XFMR signal originates in the spatially averaged dynamics of ≫10^6 Co nanomagnets. The observed sinusoidal oscillations for the Co nanomagnet ensemble, even when it is in the randomly magnetized state, show strong evidence of the presence of a STT as we discuss below. (2) The Co magnetization precesses with a phase delay relative to the Fe magnetization, which implies that the dynamics of the Co nanogranules and the NiFe spin source are not directly coupled via static exchange interaction. Instead, the dynamics of Co and NiFe may be coupled via STT.[24−27,32,36]

In addition to the STT, the microwave field[27] and the interlayer dipolar coupling field (e.g., orange peel coupling)[30]
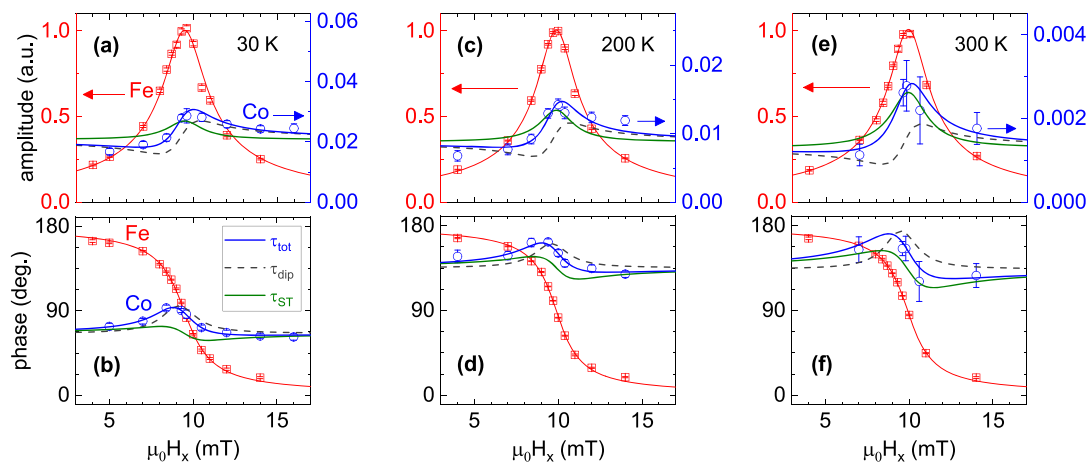

Figure 4. Field (H_x) dependence of precessional (a,c,e) amplitude and (b,d,f) phase for the NiFe spin source (Fe) and nanomagnet ensemble spin sink (Co) at (a,b) 30 K, (c,d) 200 K, and (e,f) room temperature. In each panel, the solid blue curve represents the fit with the total torque, τ_{tot}, in the Co nanomagnet ensemble, taking into account both the interlayer dipolar torque (τ_{dip}) and the STT (τ_{ST}). The dashed gray curve represents the contribution from τ_{dip} (with $\beta_{ST} = 0$ in eqs 3 and 4), and the solid green curve represents the contribution from τ_{ST} (with $\beta_{dip} = 0$ in eqs 3 and 4).

could generate additional torques that drive the precession of the Co magnetization. Although these field torques vanish in systems with zero net magnetization (Figure 1a), the net magnetization of the Co nanomagnet ensemble here is not strictly zero, due to the finite DC bias field of $\mu_0 H_x \approx 10$ mT that is necessary for inducing the FMR of NiFe. Further, while the magnetometry results (Figure 2) imply the Co nanomagnets to be superparamagnetic-like under a quasi-static field, the individual nanomagnets may be effectively in a ferromagnetic state (blocked state) at the time scale of the high-frequency AC field (e.g., 3 GHz microwave field here), as noted in the Supporting Information. We therefore must account for the possible roles of the microwave and dipolar field torques on the Co nanomagnets. On the other hand, we neglect a "field-like" STT, $\tau_{FLST} \propto -\mathbf{m}_i \times \mathbf{s}$, which cannot be readily distinguished from the microwave and dipolar field torques. This assumption of negligible field-like STT is justified, because it is typically much smaller than the conventional "damping-like" or "Slonczewski-like" STT, $\tau_{ST} \propto \mathbf{m}_i \times \mathbf{s} \times \mathbf{m}_i$, in metallic spin-valve-like stacks.[1,2]

To determine the strength of the STT relative to the microwave and dipolar field torques, we analyze the amplitude and phase of magnetization precession versus H_x. Figure 4 summarizes our XFMR measurement results at 30 K (Figure 4a,b), 200 K (Figure 4c,d), and room temperature (Figure 4e,f). The results show a clear FMR response of the NiFe spin source that is largely independent of temperature: the precessional amplitude,

$$A_{src} \propto \sqrt{\Delta H^2 / [(H_x - H_{FMR})^2 + \Delta H^2]} \tag{1}$$

exhibits a peak at the resonance field $\mu_0 H_{FMR} \approx 10$ mT with a half-width-at-half-maximum linewidth $\mu_0 \Delta H \approx 1$ mT, and the precessional phase,

$$\tan \phi_{src} = \Delta H / (H_x - H_{FMR}) \tag{2}$$

undergoes a shift of 180° across the resonance.[31]

The XFMR signal at the Co edge is more than an order of magnitude smaller, as shown in the plots of the Co amplitude normalized by the Fe amplitude (Figure 4a,c,e). It was therefore impractical to acquire sufficient signal-to-noise ratios at many values of H_x for Co within our allotted synchrotron beam time. Nevertheless, the data in Figure 4 permit us to draw quantitative conclusions about the STT on the Co nanomagnets.

First, the precessional phase for Co does not exhibit a 180° shift, which verifies the absence of Co FMR (i.e., the Co magnetization is not driven resonantly by the microwave field) near $\mu_0 H_x \approx 10$ mT. A separate FMR measurement on a 10 nm thick CoCu film indeed indicates that its 3 GHz resonance (at least an order of magnitude weaker than that of NiFe) only arises at a much higher field of $\mu_0 H_x > 50$ mT. Similar to previous XFMR experiments,[27,34,36] we therefore do not explicitly account for the FMR of the CoCu spin sink in our analysis.

We then self-consistently fit the observed amplitude A^{Co} and phase ϕ^{Co} at the Co edge with the following equations, derived from coupled Landau–Lifshitz–Gilbert equations,[27,34,36] accounting for the off-resonance microwave field torque, dipolar field torque, and STT

$$A^{Co} = A_0^{Co} \Big/ \sqrt{1 + (\beta_{dip}^2 + \beta_{ST}^2)\sin^2\phi_{src} + 2(\beta_{dip}\sin\phi_{src}\cos\phi_{src} + \beta_{ST}\sin^2\phi_{src})} \tag{3}$$

$$\tan(\phi^{Co} - \phi_0^{Co}) = \frac{\beta_{dip}\sin^2\phi_{src} - \beta_{ST}\sin\phi_{src}\cos\phi_{src}}{1 + \beta_{dip}\sin\phi_{src}\cos\phi_{src} + \beta_{ST}\sin^2\phi_{src}} \tag{4}$$

Here, A_0^{Co} is a coefficient proportional to the microwave field torque, taken to be constant in the measured range of H_x. β_{dip} and β_{ST} are coefficients that parametrize the dipolar field torque and STT, respectively, normalized by the microwave field torque.[27,36]

The dipolar field torque and STT are orthogonal to each other and hence exhibit qualitatively distinct H_x dependences. For instance, the dipolar field torque yields a precessional amplitude that is antisymmetric about $H_x = H_{FMR}$ (dashed gray curve in Figure 4a,c,e), whereas the STT yields a precessional amplitude that is symmetric about $H_x = H_{FMR}$ (solid green curve in Figure 4a,c,e). This symmetry is reversed for the precessional phase (Figure 4b,d,f): the dipolar torque (STT) generates a symmetric (antisymmetric) curve. We emphasize that while this line shape analysis may be reminiscent of the oft-used spin-torque FMR technique,[40] the XFMR method is distinct in that it directly acquires the amplitude and phase of element-specific dynamics, that is, Co magnetization in the spin sink in this case.

Figure 5 summarizes our results on the three fitting parameters (A_0^{Co}, β_{dip}, and β_{ST}) in eqs 3 and 4. The amplitude of the Co XFMR signal decreases markedly with increasing temperature (Figure 4a,c,e), as evidenced by an order of magnitude reduction in A_0^{Co} from 30 K to room temperature
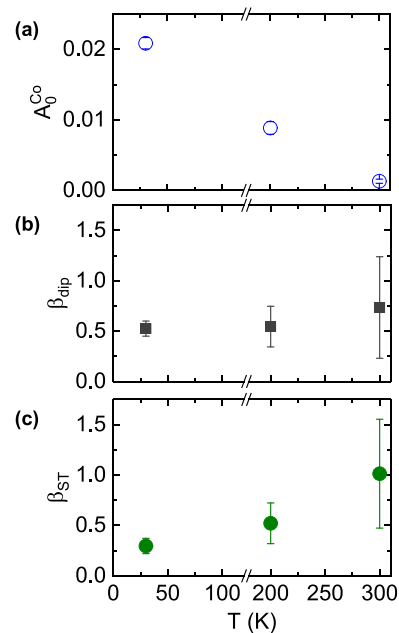

Figure 5. Temperature dependence of (a) A_0^{Co}, the coefficient proportional to the off-resonance microwave field torque, (b) β_{dip}, coefficient proportional to the ratio between the dipolar field torque and microwave field torque, and (c) β_{ST}, coefficient proportional to the ratio between the STT and microwave field torque. The error bars are derived from the 95% confidence intervals of the fit parameters in eqs 3 and 4.

(Figure 5a). This trend is partially accounted for by the reduced net magnetization of the Co nanomagnet ensemble at higher temperatures, with thermal fluctuations decreasing the vector average of the Co nanomagnet moments probed by the X-ray beam. An additional possible contribution to the reduction of A_0^{Co} (i.e., increased effective damping from thermal fluctuations[41]) is discussed in the Supporting Information. We also find that β_{dip}, which is proportional to the ratio of the dipolar field torque over the microwave field torque, remains constant within the error bars (Figure 5b). The temperature independence of β_{dip} is expected, as the microwave and dipolar field torques both depend on the net magnetization of the Co nanomagnet ensemble; when the net magnetization decreases with increasing temperature, the microwave and dipolar field torques decrease at the same rate. In the Supporting Information, we show that treating β_{dip} as a fixed parameter does not affect our key conclusion.

While the net magnetization and the field torques in the nanomagnet ensemble become small at room temperature, an enhanced role of the STT relative to the field torques is evidenced by the increase of β_{ST} with increasing temperature, as shown in Figure 5c. Recalling that β_{ST} is proportional to the ratio of the STT over the microwave field torque, the trend in Figure 5c indicates that any reduction of the global STT in the nanomagnet ensemble is modest, compared to the sharp suppression of field torques, when magnetic order diminishes at elevated temperatures. This trend is qualitatively consistent with the physical picture in Figure 1 that the global STT remains finite even in a magnetic system with null net moment.

Furthermore, our results from different temperatures verify that STT is operative regardless of whether the Co nanomagnets in the spin sink are collectively aligned or randomly magnetized; a coherent AC spin current generates a torque in each nanomagnet, resulting in a finite net torque summed over the macroscopic ensemble (Figure 1b). Our findings thus point to STT as an effective mechanism at the subnanosecond time scale to manipulate a macroscopic collection of weakly interacting nanomagnets. Such STT control of nanomagnets in unpatterned, disordered granular films (readily grown by sputtering) also has significant implications for spintronic device fabrication and integration, as it may relax the requirements on material processing (e.g., thermal budgets and additional process steps) that are generally needed to achieve crystalline epitaxy or magnetic alignment.

We finally comment on the sensitivity of the XFMR setup in our study. By comparing the amplitudes of the XFMR and static XMCD scans, we have estimated the resonant precessional cone angles. The cone angle for the FMR-driven NiFe spin source is $\approx 1.0°$, similar to prior experiments.[27,30−36] Remarkably, the average cone angle of the Co nanomagnets at room temperature is estimated to be only $\approx 0.003°$. This XFMR setup is therefore an excellent tool for examining small-angle dynamics in multilayered and multielement thin-film systems.

In summary, by employing time- and element-resolved XFMR spectroscopy,[27,34,36] we have detected an STT that is driven by a coherent 3 GHz AC spin current in a macroscopic ensemble of Co nanomagnets. We verify that the STT is able to act globally on randomly oriented nanomagnets at nanosecond time scales, even while magnetic field torques become increasingly inefficient in magnetizing these nanomagnets. Our results highlight a fundamental feature of STT,

that is, angular momentum supplied by a spin current can efficiently manipulate magnetic systems, even those with a vanishingly small global net moment. From a practical perspective, STT may form an attractive mechanism to align an ensemble of nanomagnets in the absence of applied magnetic fields, which may find uses in new information processing technologies with fewer restrictions on material processing and device preconditioning.

■ ASSOCIATED CONTENT

Ⓢ Supporting Information

The Supporting Information is available free of charge at https://pubs.acs.org/doi/10.1021/acs.nanolett.0c01868.

> Details of sample growth and structural properties; methods of magnetometry, magnetotransport, broadband ferromagnetic resonance, X-ray magnetic circular dichroism, and X-ray ferromagnetic resonance measurements; estimation of the room-temperature blocking frequency; discussion on the temperature dependence of β_{dip} and A_0^{Co}; X-ray ferromagnetic resonance measurements on a control sample with a pure Co spin sink (PDF)

■ AUTHOR INFORMATION

Corresponding Author

Satoru Emori − *Department of Physics, Virginia Tech, Blacksburg, Virginia 24061, United States;* ⓘ orcid.org/0000-0001-8035-317X; Email: semori@vt.edu

Authors

Christoph Klewe − *Advanced Light Source, Lawrence Berkeley National Laboratory, Berkeley, California 94720, United States*

Jan-Michael Schmalhorst − *Center for Spinelectronic Materials and Devices, Physics Department, Bielefeld University, 33615 Bielefeld, Germany*

Jan Krieft − *Center for Spinelectronic Materials and Devices, Physics Department, Bielefeld University, 33615 Bielefeld, Germany*

Padraic Shafer − *Advanced Light Source, Lawrence Berkeley National Laboratory, Berkeley, California 94720, United States;* ⓘ orcid.org/0000-0001-9363-2557

Youngmin Lim − *Department of Physics, Virginia Tech, Blacksburg, Virginia 24061, United States*

David A. Smith − *Department of Physics, Virginia Tech, Blacksburg, Virginia 24061, United States*

Arjun Sapkota − *Department of Physics and Astronomy, University of Alabama, Tuscaloosa, Alabama 35487, United States*

Abhishek Srivastava − *Department of Physics and Astronomy, University of Alabama, Tuscaloosa, Alabama 35487, United States*

Claudia Mewes − *Department of Physics and Astronomy, University of Alabama, Tuscaloosa, Alabama 35487, United States*

Zijian Jiang − *Department of Physics, Virginia Tech, Blacksburg, Virginia 24061, United States*

Behrouz Khodadadi − *Department of Physics, Virginia Tech, Blacksburg, Virginia 24061, United States*

Hesham Elmkharram − *Department of Materials Science and Engineering, Virginia Tech, Blacksburg, Virginia 24061, United States*

Jean J. Heremans − *Department of Physics, Virginia Tech, Blacksburg, Virginia 24061, United States;* ● orcid.org/0000-0002-6346-8597

Elke Arenholz − *Advanced Light Source, Lawrence Berkeley National Laboratory, Berkeley, California 94720, United States; Cornell High Energy Synchrotron Source, Ithaca, New York 14853, United States*

Günter Reiss − *Center for Spinelectronic Materials and Devices, Physics Department, Bielefeld University, 33615 Bielefeld, Germany*

Tim Mewes − *Department of Physics and Astronomy, University of Alabama, Tuscaloosa, Alabama 35487, United States*

Complete contact information is available at:
https://pubs.acs.org/10.1021/acs.nanolett.0c01868

Notes
The authors declare no competing financial interest.

◼ REFERENCES

(1) Ralph, D. C.; Stiles, M. D. Spin Transfer Torques. *J. Magn. Magn. Mater.* **2008**, *320* (7), 1190−1216.

(2) Brataas, A.; Kent, A. D.; Ohno, H. Current-Induced Torques in Magnetic Materials. *Nat. Mater.* **2012**, *11* (5), 372−381.

(3) Manchon, A.; Železný, J.; Miron, I. M.; Jungwirth, T.; Sinova, J.; Thiaville, A.; Garello, K.; Gambardella, P. Current-Induced Spin-Orbit Torques in Ferromagnetic and Antiferromagnetic Systems. *Rev. Mod. Phys.* **2019**, *91* (3), 35004.

(4) Locatelli, N.; Cros, V.; Grollier, J. Spin-Torque Building Blocks. *Nat. Mater.* **2014**, *13* (1), 11−20.

(5) Sander, D.; Valenzuela, S. O.; Makarov, D.; Marrows, C. H.; Fullerton, E. E.; Fischer, P.; McCord, J.; Vavassori, P.; Mangin, S.; Pirro, P.; et al. The 2017 Magnetism Roadmap. *J. Phys. D: Appl. Phys.* **2017**, *50* (36), 363001.

(6) Watanabe, K.; Jinnai, B.; Fukami, S.; Sato, H.; Ohno, H. Shape Anisotropy Revisited in Single-Digit Nanometer Magnetic Tunnel Junctions. *Nat. Commun.* **2018**, *9* (1), 663.

(7) Borders, W. A.; Pervaiz, A. Z.; Fukami, S.; Camsari, K. Y.; Ohno, H.; Datta, S. Integer Factorization Using Stochastic Magnetic Tunnel Junctions. *Nature* **2019**, *573* (7774), 390−393.

(8) Železný, J.; Gao, H.; Výborný, K.; Zemen, J.; Mašek, J.; Manchon, A.; Wunderlich, J.; Sinova, J.; Jungwirth, T. Relativistic Néel-Order Fields Induced by Electrical Current in Antiferromagnets. *Phys. Rev. Lett.* **2014**, *113* (15), 157201.

(9) Wadley, P.; Howells, B.; Elezny, J.; Andrews, C.; Hills, V.; Campion, R. P.; Novak, V.; Olejnik, K.; Maccherozzi, F.; Dhesi, S. S.; Martin, S. Y.; Wagner, T.; Wunderlich, J.; Freimuth, F.; Mokrousov, Y.; Kune, J.; Chauhan, J. S.; Grzybowski, M. J.; Rushforth, A. W.; Edmonds, K. W.; Gallagher, B. L.; Jungwirth, T. Electrical Switching of an Antiferromagnet. *Science (Washington, DC, U. S.)* **2016**, *351* (6273), 587.

(10) Cheng, R.; Xiao, D.; Brataas, A. Terahertz Antiferromagnetic Spin Hall Nano-Oscillator. *Phys. Rev. Lett.* **2016**, *116* (20), 207603.

(11) Khymyn, R.; Lisenkov, I.; Tiberkevich, V.; Ivanov, B. A.; Slavin, A. Antiferromagnetic THz-Frequency Josephson-like Oscillator Driven by Spin Current. *Sci. Rep.* **2017**, *7*, 43705.

(12) Parks, B.; Bapna, M.; Igbokwe, J.; Almasi, H.; Wang, W.; Majetich, S. A. Superparamagnetic Perpendicular Magnetic Tunnel Junctions for True Random Number Generators. *AIP Adv.* **2018**, *8* (5), 055903.

(13) Lv, Y.; Bloom, R. P.; Wang, J.-P. Experimental Demonstration of Probabilistic Spin Logic by Magnetic Tunnel Junctions. *IEEE Magn. Lett.* **2019**, *10*, 1.

(14) Skomski, R.; Zhou, J.; Istomin, A. Y.; Starace, A. F.; Sellmyer, D. J. Magnetic Materials for Finite-Temperature Quantum Computing. *J. Appl. Phys.* **2005**, *97* (10), 10R511.

(15) Dorroh, D. D.; Ölmez, S.; Wang, J.-P. Theory of Quantum Computation With Magnetic Clusters. *IEEE Trans. Quantum Eng.* **2020**, *1*, 5100508.

(16) Mewes, C. K. A.; Mewes, T. Relaxation in Magnetic Materials for Spintronics. In *Handbook of Nanomagnetism: Applications and Tools*; Pan Stanford, 2015; pp 71−95.

(17) Krause, S.; Berbil-Bautista, L.; Herzog, G.; Bode, M.; Wiesendanger, R. Current-Induced Magnetization Switching with a Spin-Polarized Scanning Tunneling Microscope. *Science (Washington, DC, U. S.)* **2007**, *317* (5844), 1537−1540.

(18) Kiselev, S. I.; Sankey, J. C.; Krivorotov, I. N.; Emley, N. C.; Garcia, A. G. F.; Buhrman, R. A.; Ralph, D. C. Spin-Transfer Excitations of Permalloy Nanopillars for Large Applied Currents. *Phys. Rev. B: Condens. Matter Mater. Phys.* **2005**, *72* (6), 64430.

(19) Bapna, M.; Majetich, S. A. Current Control of Time-Averaged Magnetization in Superparamagnetic Tunnel Junctions. *Appl. Phys. Lett.* **2017**, *111* (24), 243107.

(20) Mizrahi, A.; Hirtzlin, T.; Fukushima, A.; Kubota, H.; Yuasa, S.; Grollier, J.; Querlioz, D. Neural-like Computing with Populations of Superparamagnetic Basis Functions. *Nat. Commun.* **2018**, *9* (1), 1533.

(21) Chen, T. Y.; Huang, S. X.; Chien, C. L.; Stiles, M. D. Enhanced Magnetoresistance Induced by Spin Transfer Torque in Granular Films with a Magnetic Field. *Phys. Rev. Lett.* **2006**, *96* (20), 207203.

(22) Luo, Y.; Esseling, M.; Münzenberg, M.; Samwer, K. A Novel Spin Transfer Torque Effect in Ag_2 Co Granular Films. *New J. Phys.* **2007**, *9* (9), 329−329.

(23) Wang, X. J.; Zou, H.; Ji, Y. Spin Transfer Torque Switching of Cobalt Nanoparticles. *Appl. Phys. Lett.* **2008**, *93* (16), 162501.

(24) Tserkovnyak, Y.; Brataas, A.; Bauer, G. Spin Pumping and Magnetization Dynamics in Metallic Multilayers. *Phys. Rev. B: Condens. Matter Mater. Phys.* **2002**, *66* (22), 224403.

(25) Heinrich, B.; Tserkovnyak, Y.; Woltersdorf, G.; Brataas, A.; Urban, R.; Bauer, G. E. W. Dynamic Exchange Coupling in Magnetic Bilayers. *Phys. Rev. Lett.* **2003**, *90* (18), 187601.

(26) Ghosh, A.; Auffret, S.; Ebels, U.; Bailey, W. E. Penetration Depth of Transverse Spin Current in Ultrathin Ferromagnets. *Phys. Rev. Lett.* **2012**, *109* (12), 127202.

(27) Li, J.; Shelford, L. R.; Shafer, P.; Tan, A.; Deng, J. X.; Keatley, P. S.; Hwang, C.; Arenholz, E.; van der Laan, G.; Hicken, R. J.; et al. Direct Detection of Pure Ac Spin Current by X-Ray Pump-Probe Measurements. *Phys. Rev. Lett.* **2016**, *117* (7), 76602.

(28) Xiao, J. Q.; Jiang, J. S.; Chien, C. L. Giant Magnetoresistance in Nonmultilayer Magnetic Systems. *Phys. Rev. Lett.* **1992**, *68* (25), 3749−3752.

(29) Berkowitz, A. E.; Mitchell, J. R.; Carey, M. J.; Young, A. P.; Zhang, S.; Spada, F. E.; Parker, F. T.; Hutten, A.; Thomas, G. Giant Magnetoresistance in Heterogeneous Cu-Co Alloys. *Phys. Rev. Lett.* **1992**, *68* (25), 3745−3748.

(30) Arena, D. A.; Vescovo, E.; Kao, C.-C.; Guan, Y.; Bailey, W. E. Weakly Coupled Motion of Individual Layers in Ferromagnetic Resonance. *Phys. Rev. B: Condens. Matter Mater. Phys.* **2006**, *74* (6), 64409.

(31) Guan, Y.; Bailey, W. E.; Vescovo, E.; Kao, C.-C.; Arena, D. A. Phase and Amplitude of Element-Specific Moment Precession in Ni81Fe19. *J. Magn. Magn. Mater.* **2007**, *312* (2), 374−378.

(32) Marcham, M. K.; Shelford, L. R.; Cavill, S. A.; Keatley, P. S.; Yu, W.; Shafer, P.; Neudert, A.; Childress, J. R.; Katine, J. A.; Arenholz, E.; et al. Phase-Resolved X-Ray Ferromagnetic Resonance Measurements of Spin Pumping in Spin Valve Structures. *Phys. Rev. B: Condens. Matter Mater. Phys.* **2013**, *87* (18), 180403.

(33) Stenning, G B G; Shelford, L R; Cavill, S A; Hoffmann, F; Haertinger, M; Hesjedal, T; Woltersdorf, G; Bowden, G J; Gregory, S A; Back, C H; Groot, P A J d.; van der Laan, G. Magnetization Dynamics in an Exchange-Coupled NiFe/CoFe Bilayer Studied by X-Ray Detected Ferromagnetic Resonance. *New J. Phys.* **2015**, *17* (1), 013019.

(34) Baker, A. A.; Figueroa, A. I.; Love, C. J.; Cavill, S. A.; Hesjedal, T.; van der Laan, G. Anisotropic Absorption of Pure Spin Currents. *Phys. Rev. Lett.* **2016**, *116* (4), 47201.

(35) Durrant, C. J.; Shelford, L. R.; Valkass, R. A. J.; Hicken, R. J.; Figueroa, A. I.; Baker, A. A.; van der Laan, G.; Duffy, L. B.; Shafer, P.; Klewe, C.; et al. Dependence of Spin Pumping and Spin Transfer Torque upon $Ni_{81}Fe_{19}$ Thickness in $Ta/Ag/Ni_{81}Fe_{19}/Ag/Co_2MnGe/Ag/Ta$ Spin-Valve Structures. *Phys. Rev. B: Condens. Matter Mater. Phys.* **2017**, *96* (14), 144421.

(36) Li, Q.; Yang, M.; Klewe, C.; Shafer, P.; N'Diaye, A. T.; Hou, D.; Wang, T. Y.; Gao, N.; Saitoh, E.; Hwang, C.; et al. Coherent Ac Spin Current Transmission across an Antiferromagnetic CoO Insulator. *Nat. Commun.* **2019**, *10* (1), 5265.

(37) Leal, J. L.; Kryder, M. H. Oscillatory Interlayer Exchange Coupling in $Ni_{81}Fe_{19}/Cu/Ni_{81}Fe_{19}/Fe_{50}Mn_{50}$ Spin Valves. *J. Appl. Phys.* **1996**, *79* (5), 2801−2803.

(38) Schoen, M. A. W.; Lucassen, J.; Nembach, H. T.; Silva, T. J.; Koopmans, B.; Back, C. H.; Shaw, J. M. Magnetic Properties in Ultrathin 3d Transition-Metal Binary Alloys. II. Experimental Verification of Quantitative Theories of Damping and Spin Pumping. *Phys. Rev. B: Condens. Matter Mater. Phys.* **2017**, *95* (13), 134411.

(39) Zhao, Y.; Song, Q.; Yang, S.-H.; Su, T.; Yuan, W.; Parkin, S. S. P.; Shi, J.; Han, W. Experimental Investigation of Temperature-Dependent Gilbert Damping in Permalloy Thin Films. *Sci. Rep.* **2016**, *6*, 22890.

(40) Liu, L.; Moriyama, T.; Ralph, D. C.; Buhrman, R. A. Spin-Torque Ferromagnetic Resonance Induced by the Spin Hall Effect. *Phys. Rev. Lett.* **2011**, *106* (3), 36601.

(41) Chubykalo-Fesenko, O.; Nowak, U.; Chantrell, R. W.; Garanin, D. Dynamic Approach for Micromagnetics close to the Curie Temperature. *Phys. Rev. B: Condens. Matter Mater. Phys.* **2006**, *74* (9), 94436.

SUPPORTING INFORMATION:

Element-Specific Detection of Sub-Nanosecond Spin-Transfer Torque in a Nanomagnet Ensemble

Satoru Emori[1], Christoph Klewe[2], Jan-Michael Schmalhorst[3], Jan Krieft[3], Padraic Shafer[2], Youngmin Lim[1], David A. Smith[1], Arjun Sapkota[4,5], Abhishek Srivastava[4,5], Claudia Mewes[4,5], Zijian Jiang[1], Behrouz Khodadadi[1], Hesham Elmkharram[6], Jean J. Heremans[1], Elke Arenholz[2,7], Gunter Reiss[3], Tim Mewes[4,5]

1. Department of Physics, Virginia Tech, Blacksburg, VA 24061, USA

2. Advanced Light Source, Lawrence Berkeley National Laboratory, Berkeley, CA 94720, USA

3. Center for Spinelectronic Materials & Devices, Physics Department, Bielefeld University, Universitätsstraße 25, 33615 Bielefeld, Germany

4. Department of Physics and Astronomy, University of Alabama, Tuscaloosa, AL 35487, USA

5. Center for Materials for Information Technology (MINT), University of Alabama, Tuscaloosa, AL 35487, USA

6. Department of Materials Science and Engineering, Virginia Tech, Blacksburg, VA 24061, USA

7. Cornell High Energy Synchrotron Source, Ithaca, NY 14853, USA

I. Sample Details

In the Letter, we show results from two film structures: subs./$Co_{25}Cu_{75}$(10)/Al(2) and subs./$Ni_{80}Fe_{20}$(10)/ Cu(5)/$Co_{25}Cu_{75}$(10)/Al(2), where the values in the parentheses denote nominal layer thicknesses in nm. The Al(2) capping layer protects each sample from oxidation, and the Cu(5) spacer layer suppresses static exchange coupling between the NiFe and CoCu layers. All films were grown in the same DC sputter deposition system, with substrates at room temperature (no active heating or cooling). NiFe was sputtered from a single stoichiometric target, whereas CoCu was grown by co-sputtering Co and Cu targets. Each film structure was deposited on two types of substrates (subs.) simultaneously: (001)-oriented MgO single crystal and (001)-oriented Si wafer with native oxide. No post-annealing was performed. Films deposited on both substrates are polycrystalline (as verified by powder X-ray diffraction and transmission electron microscopy) and exhibit essentially identical magnetic properties. Results shown in the letter are obtained on films on MgO substrate, as MgO strongly when irradiated by soft X-rays and therefore enables high luminescence yield signals for X-ray magnetic circular dichroism and X-ray ferromagnetic resonance measurements (explained later). To deduce the average grain size from powder X-ray diffraction, we measured CoCu on Si, which had significantly fewer substrate peaks than CoCu on MgO and thus simplified the analysis.

We have attempted element-resolved transmission electron microscopy on our CoCu films, but were unable to acquire micrographs with sufficient resolution to confirm the distribution of Co and Cu. Nevertheless, our $Co_{25}Cu_{75}$ films are likely to be granular for the following reasons: (1) the magnetoresistance loops (shown in Fig. 2 of the main text) strongly resemble those reported previously for typical granular films; and (2) the percolation limit for the FCC CoCu lattice is 19.8 at%[1].

II. Magnetometry and Magnetotransport Measurements

Vibrating sample magnetometry was performed at room temperature using a Microsense EZ9 VSM. Magnetotransport measurements, with each sample connected in a 4-point van der Pauw configuration, were carried out in a custom setup equipped with a cryostat and electromagnet.

III. Broadband Ferromagnetic Resonance (FMR) Measurements

FMR measurements were performed on a coplanar-waveguide-based spectrometer equipped with a cryostat and electromagnet. The sample was magnetized in-plane. FMR spectra were acquired via field modulation to obtain the peak-to-peak FMR linewidth ΔH_{pp} of the NiFe layer at frequencies in the range 3-40 GHz. From the linear frequency dependence of the ΔH_{pp}, the Gilbert damping parameter α is obtained using[2]

$$\mu_0 \Delta H_{pp} = \mu_0 \Delta H_{pp,0} + \frac{2}{\sqrt{3}} \frac{2\pi}{\gamma} \alpha f, \qquad (S1)$$

where μ_0 is the permeability of free space, $\Delta H_{pp,0}$ is the zero-frequency inhomogeneous linewidth broadening, and $\frac{\gamma}{2\pi} \approx 29$ GHz/T is the gyromagnetic ratio.

IV. X-ray Magnetic Circular Dichroism (XMCD) and X-ray Ferromagnetic Resonance (XFMR) Measurements

XMCD and XFMR (i.e., pump-probe dynamic XMCD) measurements were performed on Beamline 4.0.2 at the Advanced Light Source, Lawrence Berkeley National Laboratory[3,4]. Both measurements were performed by mounting the MgO(subs.)/NiFe/Cu/CoCu/Al sample on a coplanar waveguide (CPW), with the film side facing the CPW. A tapered hole in the center conductor of the CPW allows the X-ray beam (circular polarization of 90%) to reach the sample

with an incident angle of 50° with respect to the film normal. The XMCD signal is collected with a photodiode by monitoring the X-ray induced luminescence of the MgO substrate. The Fe L_3 edge and Co L_3 edge signals were collected at nominal X-ray photon energies of 706.5 eV and 777.2 eV, respectively. Static XMCD magnetization curves (Fig. 2(c,d)) were measured with a magnetic field swept in the film plane. For XFMR measurements, a microwave field was delivered via the CPW to drive precessional magnetization dynamics, such that the time-varying in-plane transverse magnetization component could be detected by XMCD. To ensure a fixed phase relation between the microwave excitation and the probing X-ray pulses (pulse width ≈70 ps), the microwave is generated as a higher harmonic of the 500 MHz master oscillator of the storage ring. In our experiments the 6th harmonic of the master oscillator, i.e., 3 GHz, was used for the microwave frequency. The microwave excitation is phase modulated at 333 Hz between 0° and 180° and the XFMR signal is acquired stroboscopically as the difference in the X-ray absorption for the opposing magnetization states on the precession cone. The photodiode output is evaluated with a lock-in amplifier. At a fixed bias magnetic field H_x, by incrementally delaying the phase of the microwave excitation with respect to the phase of the X-ray pulses, the complete magnetization precession cycle can be mapped (example shown in Fig. 3(d)).

V. Estimation of the Blocking Frequency at Room Temperature

The Co nanomagnets in the CoCu sink are superparamagnetic-like at room temperature at the time scale of DC magnetometry measurements. However, these nanomagnets may effectively be in a ferromagnetic state (blocked state) at a much shorter time scale (higher frequency), e.g., <1 ns in our GHz-range FMR measurements. The average frequency of the flipping of the nanomagnet magnetization by thermal fluctuations is estimated by $f_N = f_0 e^{-\frac{KV}{k_B T}}$, where f_0 is the

attempt frequency, K is the magnetic anisotropy energy density, V is the volume of the nanomagnet, and $k_B T$ is the thermal energy. The attempt frequency is typically taken to be on the order of ~10^9 s^{-1}. If the nanomagnets were perfectly isotropic ($K = 0$), the blocking frequency would also be expected to be ~10^9 s^{-1}. Thus, the individual nanomagnets would be essentially in a blocked state (i.e., not in a superparamagnetic-like state) at the time scale of the 3-GHz microwave excitation used in our FMR experiment. If modest magnetic anisotropy (e.g., $K = 10^4$ J/m^3) were assumed for the nanomagnets, with an approximate volume of $V = (10 \text{ nm})^3 = 10^{-24}$ m^3, the frequency above which the nanomagnets are blocked would be ~10^8 s^{-1}. In this case, it would be even more likely for the individual nanomagnets to be in a blocked state at the time scale of our FMR experiment.

VI. Temperature Dependence of β$_{dip}$

In the main text, β$_{dip}$ was assumed to be a free fit parameter. We have also performed fits using Equations 2 and 3 with β$_{dip}$ as a fixed parameter, assumed to be constant with temperature at $\beta_{dip} = 0.53 +/- 0.08$, derived from the results at 30 K (Fig. 4(a,b)). The temperature dependent results for the other free fit parameters, A_0^{Co} and β$_{ST}$, are almost the same with β$_{dip}$ as a free parameter (Fig. S1(a)) or β$_{dip}$ as a fixed parameter (Fig. S1(b)).
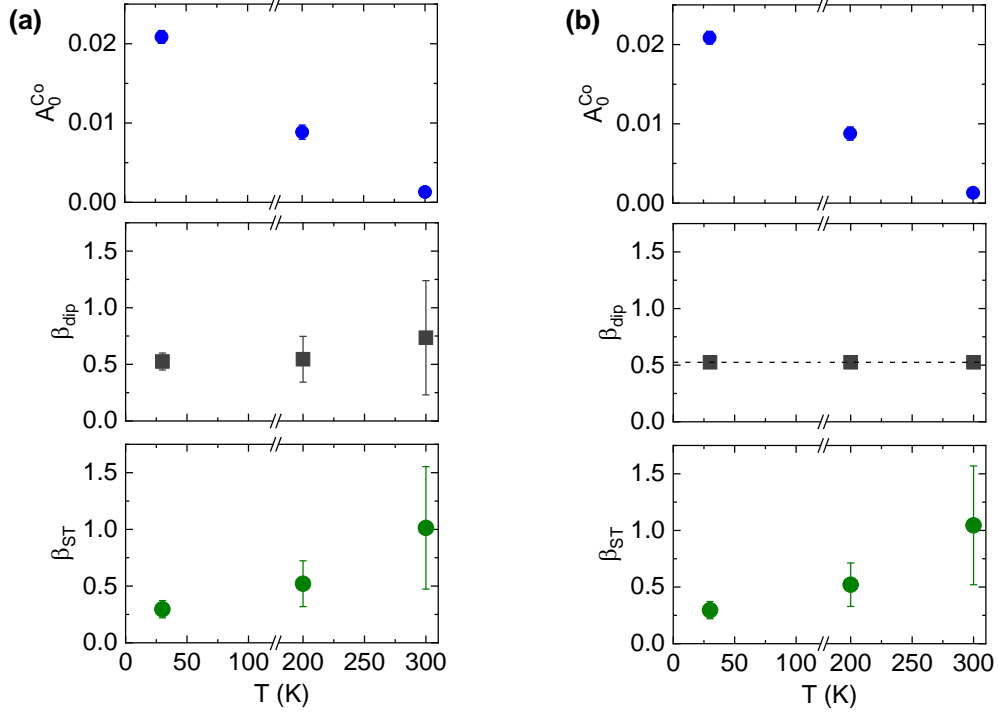
Figure S1.

VII. Temperature Dependence of A_0^{Co}

The amplitude of the Co XFMR signal decreases markedly with increasing temperature (Fig. 4(a,c,e), main text), as evidenced by an order of magnitude reduction in A_0^{Co} from 30 K to room temperature (Fig. 5(a), main text). This trend is partially accounted for by the reduced net magnetization of the Co nanomagnet ensemble at higher temperatures. However, our XMCD magnetometry results (Fig. 2(c,d)) suggest that the Co net magnetization at $\mu_0 H_x$ ~10 mT decreases by only a factor of ≈4 between 30 K and room temperature, such that there is likely an additional contribution to the ≈10-fold decrease of A_0^{Co}. We speculate that the Co nanomagnets (CoCu spin sink) have higher effective damping at room temperature than at 30 K. The higher damping decreases the average cone angle of the Co moments driven by a given amount of microwave field (along with dipolar field and spin current), hence further reducing A_0^{Co} at higher

temperature. Prior theoretical work has suggests higher effective damping can result from enhanced thermal fluctuations (e.g., in magnetic materials approaching the Curie temperature)[5].

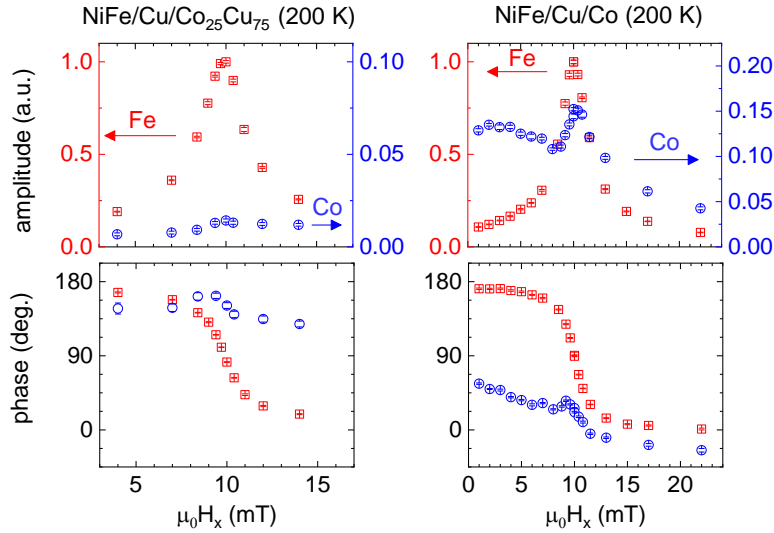## VIII. XFMR of a Control Sample with a Pure Co Spin Sink

Figure S2.

We have performed XFMR measurements on a MgO/Ni$_{80}$Fe$_{20}$(10)/Cu(5)/Co(2.5)/Al(2) stack, where the pure ferromagnetic Co layer acts as the spin sink. Figure S2 compares the field dependence of the amplitude and phase data (acquired at 3 GHz, 200 K) for this pure Co spin sink sample and the CoCu (Co nanomagnet ensemble) spin sink shown in the main text. The pure Co sink sample shows the characteristic signature of spin-transfer torque – namely, the symmetric (antisymmetric) peak in amplitude (phase) corresponding to the resonance field of the NiFe spin source at $\mu_0 H_x \approx 10$ mT. This is qualitatively similar to the results from the CoCu sink sample. However, there are a few major differences between the Co and CoCu sink samples:

- The Co sample shows a much higher amplitude at the Co edge than the CoCu sample, consistent with the much larger net magnetization of the pure ferromagnetic Co sink than the weakly interacting ensemble of Co nanomagnets in the CoCu sink.

- The Co sample exhibits a broad yet clear FMR response at the Co edge centered around $\mu_0 H_x \approx 2$ mT, whereas no Co FMR is evident for the CoCu sample. (Separate broadband FMR measurements indicate 3-GHz FMR for CoCu appears at >50 mT.)

- The baseline phase at the Co edge is lower for the pure ferromagnetic Co sink than the low net-moment CoCu sink. This is qualitatively consistent with what is presented in the main text (Fig. 4): the baseline phase is lowered with increasing net magnetization as the global magnetization of the Co nanomagnets in the CoCu sink transitions from a randomly magnetized state to a collectively aligned state at low temperature.

References cited in this Supporting Information

(1)   Stauffer, D.; Aharony, A. *Perkolationstheorie: Eine Einführung*; Wiley-VCH, 1995.

(2)   Mewes, C. K. A.; Mewes, T. Relaxation in Magnetic Materials for Spintronics. In *Handbook of Nanomagnetism: Applications and Tools*; Pan Stanford, 2015; pp 71–95.

(3)   Li, J.; Shelford, L. R.; Shafer, P.; Tan, A.; Deng, J. X.; Keatley, P. S.; Hwang, C.; Arenholz, E.; van der Laan, G.; Hicken, R. J.; et al. Direct Detection of Pure Ac Spin Current by X-Ray Pump-Probe Measurements. *Phys. Rev. Lett.* **2016**, *117* (7), 76602. https://doi.org/10.1103/PhysRevLett.117.076602.

(4)   Li, Q.; Yang, M.; Klewe, C.; Shafer, P.; N'Diaye, A. T.; Hou, D.; Wang, T. Y.; Gao, N.; Saitoh, E.; Hwang, C.; et al. Coherent Ac Spin Current Transmission across an Antiferromagnetic CoO Insulator. *Nat. Commun.* **2019**, *10* (1), 5265. https://doi.org/10.1038/s41467-019-13280-5.

(5)   Chubykalo-Fesenko, O.; Nowak, U.; Chantrell, R. W.; Garanin, D. Dynamic Approach for Micromagnetics close to the Curie Temperature. *Phys. Rev. B* **2006**, *74* (9), 94436. https://doi.org/10.1103/PhysRevB.74.094436.